AIAA JOURNAL
Vol. 34, No. 4, April 1996

Experimental Study of a Compressible Countercurrent Turbulent Shear Layer

F. S. Alvi,* A. Krothapalli,† and D. Washington‡
Florida A&M University and Florida State University, Tallahassee, Florida 32316-2175

A countercurrent shear layer with a nominal convective Mach number (M_c) of 2 is generated using a unique arrangement. The shear layer growth rates were found to be twice that of conventional, coflowing shear layers at comparable M_c. It is hypothesized that the countercurrent shear layer becomes self-excited, leading to a modification of the turbulent properties. Instantaneous flow visualization images clearly reveal the presence of large, highly convoluted, turbulent structures believed to be responsible for the enhanced growth rates. The flowfield was also examined for the presence of eddy shocklets that have been observed in numerical simulations under similar compressible flow conditions. Even though the countercurrent flowfield appears to satisfy the criteria for the creation of shocklets, a careful and thorough search revealed no evidence of their presence.

Introduction

In recent years, the mixing characteristics of compressible shear layers have been the subject of intensive research. This is primarily the result of the limitations they impose upon the performance of air-breathing supersonic propulsion systems. Classic studies of turbulent shear layers by Brown and Roshko[1] and Papamoschou and Roshko[2] have afforded considerable insight into the behavior of compressible, turbulent shear layers. Based upon their extensive study, Papamoschou and Roshko[2] confirmed that the compressibility effect is fundamentally responsible for the reduced mixing in such shear layers. A compressibility parameter called the convective Mach number M_c, originally proposed by Bogdanoff,[3] appeared, to a large extent, to account for compressibility effects in coflowing shear layers.

Although the convective Mach number effectively unifies a large body of experimental results, recent studies by Papamoschou[4] and Bunyajitradulya and Papamoschou,[5] among others, have shown that the concept of a single convective Mach number may not be universally applicable. Several hypotheses for the behavior of compressible shear layers have been proposed.[6–8] Clemens and Mungul[6] and Shau et al.[7] noticed a transition from highly organized, two-dimensional structures to irregular, three-dimensional structures, as the convective Mach number was increased. They suggested that this evolution in dimensionality of the large-scale turbulence may be partially responsible for the reduction in mixing. Jackson and Grosch[8] investigated the stability characteristics of compressible shear layers and discovered that the amplification rates of a certain family of instability waves approached a constant value as M_c was increased, a trend similar to the experimentally observed mixing rate behavior of compressible shear layers. From the preceding discussion it is clear that a unifying theory, which explains the underlying physical mechanisms governing compressible mixing, still remains elusive.

Several studies have been undertaken to address the practical need to enhance compressible mixing. Previous attempts at mixing enhancement have been wide and varied. They range from geometric modifications to either the splitter plate trailing edge[9] or the supersonic nozzles used to generate compressible shear layers,[10] to introducing swirl and streamwise vorticity into the flow,[10,11] to the acoustic excitation of the shear layer instabilities.[12] To the authors' knowledge none of these experiments, which almost exclusively concentrated on coflowing shear layers, were able to significantly augment mixing without an associated drawback. Any appreciable enhancement in mixing was invariably associated with a penalty on performance, such as significant thrust loss in supersonic jets. Clearly a more novel approach is needed.

Countercurrent Shear Layers

Recently, Strykowski et al.[13] employed an innovative approach to generate an axisymmetric countercurrent shear layer, a mixing layer in which the two freestreams are in opposing directions in the laboratory frame of reference. Their results demonstrated that the mixing rates in the countercurrent shear layer at $M_c = 0.82$ were significantly higher (by as much as 60%) than the corresponding coflowing shear layer at the same convective Mach number. In addition to the simplicity of implementing this technique, the elevated levels of shear were achieved without any appreciable loss in thrust.

Parameters that primarily determine the development of countercurrent shear layers include the density ratio $S = \rho_2/\rho_1$, the convective Mach number $M_c = (U_1 - U_2)/(a_1 + a_2)$, and the velocity ratio $R = (U_1 - U_2)/(U_1 + U_2)$, where the subscripts denote the two freestreams. Studies[14] have shown that the plane coflowing shear layer is convectively unstable at all density ratios and values of M_c. In contrast, if the velocity ratio is increased above unity, a state only possible in countercurrent shear layers, the shear layer can become absolutely unstable. Very briefly, a convectively unstable flow is one in which the amplified instability waves have a group velocity at which they are convected away from the source of the disturbance. In contrast, in an absolutely unstable flowfield, instability waves can remain stationary in space but experience amplification with time.[15] If a finite region of the velocity field is absolutely unstable, then the flow may become self-excited,[16] which could lead to enhanced mixing rates such as those observed in counterflowing shear layers. For a more detailed discussion of stability issues, the interested reader is referred to Refs. 13–16.

The enhanced mixing in countercurrent shear layers and the potential applications based on this enhancement make the study of this flowfield particularly attractive from a practical perspective (see Ref. 13 for the application of counterflow in thrust vectoring). The relatively unexplored fluid dynamics and the possibility of an inherently different instability mechanism governing the growth of counterflowing shear layers makes this a challenging fluid dynamics problem.

The primary goal of the present work is to extend the convective Mach number range of the previous study[13] to $M_c \approx 2$, to characterize the behavior of this highly compressible countercurrent shear

Presented as Paper 95-0580 at the AIAA 33rd Aerospace Sciences Meeting, Reno, NV, Jan. 9–12, 1995; received Feb. 28, 1995; revision received Sept. 28, 1995; accepted for publication Oct. 9, 1995.

*Visiting Assistant Professor, Fluid Mechanics Research Laboratory, Department of Mechanical Engineering. Member AIAA.

†Don Fuqua Professor and Departmental Chairman, Fluid Mechanics Research Laboratory, Department of Mechanical Engineering. Associate Fellow AIAA.

‡Graduate Research Assistant, Fluid Mechanics Research Laboratory, Department of Mechanical Engineering.

layer and to study the flow physics governing its behavior. One of the crucial questions to be answered is whether the significant enhancement in mixing achieved in countercurrent shear layers at $M_c \approx 0.82$ can be observed at higher convective Mach numbers. In addition to our primary test case with maximum counterflow (i.e., $M_c \approx 2$, countercurrent shear layer) the effect of varying the degree of counterflow on shear layer mixing characteristics is explored in some detail. A brief discussion of the possible physical mechanism responsible for this behavior is also provided.

A secondary objective was to experimentally verify the existence of eddy shocklets in highly turbulent compressible shear layers. Direct numerical simulations by Lee et al.[17] have demonstrated the existence of these shocklets in highly turbulent flowfields. Their results show a marked increase in the compressible turbulence dissipation in the vicinity of the shocklets. It has been suggested that the increase in dissipation may be partially responsible for the reduction in the mixing rates of compressible shear layers.[18] Although eddy shocklets have been found in numerical simulations, to the authors' knowledge no conclusive experimental evidence of their existence is currently available. The current flowfield would meet the necessary requirements, as stipulated by Lee et al.,[17] for the generation of eddy shocklets. To this end, we explored our flowfield for eddy shocklets via highly detailed flow visualization experiments.

Experimental Facility and Techniques

Facility

The experiments were conducted in a newly constructed facility, specifically built to produce an $M_c \approx 2$ countercurrent shear layer. An abbreviated sketch of the test facility is shown in Fig. 1. Two rectangular nozzles with straight side walls and an exit aspect ratio of 6.5 (5 × 32.5 mm) were designed using a method of characteristics approach to produce a Mach 2, two-dimensional, ideally expanded flow. A settling chamber upstream of the converging section of the nozzles is equipped with a set of flow-conditioning screens and pressure and temperature ports for monitoring the stagnation conditions. To facilitate subsequent presentation and discussion of results at various test conditions, all relevant parameters, such as the vertical and horizontal jet separation (S and D, respectively), the Cartesian coordinate frame, etc., have been clearly labeled in Fig. 1.

The jets can be operated continuously in blowdown mode for approximately 20 min, thus providing ample test times. The nominal test conditions for producing ideally expanded Mach 2 flow in ambient air (101 kPa) are as follows: jet exit Mach number = 2, stagnation (total) pressure = 793 kPa, total temperature = 290–300 K (temperature drops slowly during a long test), and unit Reynolds number = 100 × 10^6. All the values are based on the jet potential core properties.

Figure 2 depicts a flowfield schematic and a time-averaged schlieren image of the countercurrent shear layer. As seen in the figure, the nozzles are positioned in opposing directions and the vertical distance (y direction) between them is adjusted such that the opposing shear layers, produced by the two counterflowing Mach 2 free jets, just graze each other. In this way, we are able to produce a two-dimensional, countercurrent shear layer with high mean shear and a nominal convective Mach number of 2. This arrangement also allows us to vary the distance between the two shear layers,

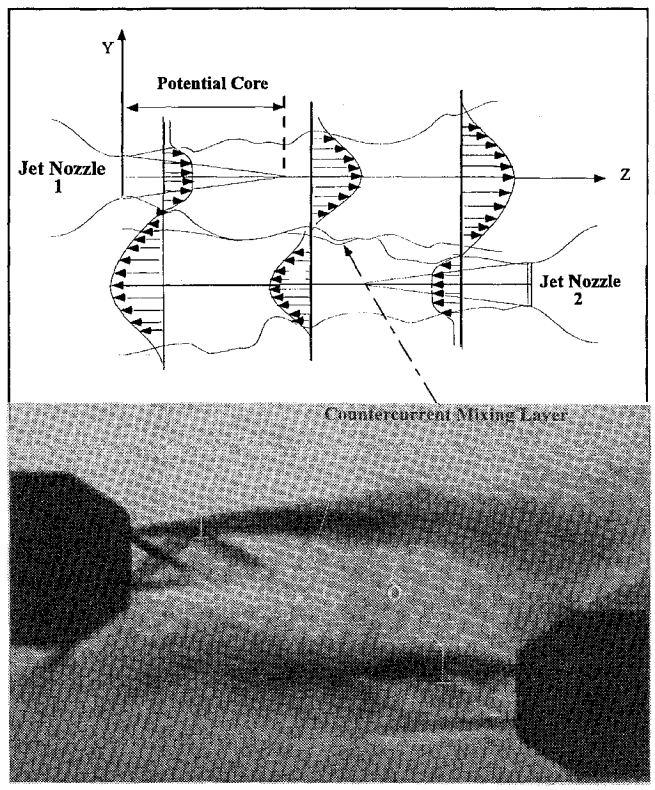

Fig. 2 Flowfield schematic and time-averaged schlieren image of $M_c \approx 2$ countercurrent shear layer.

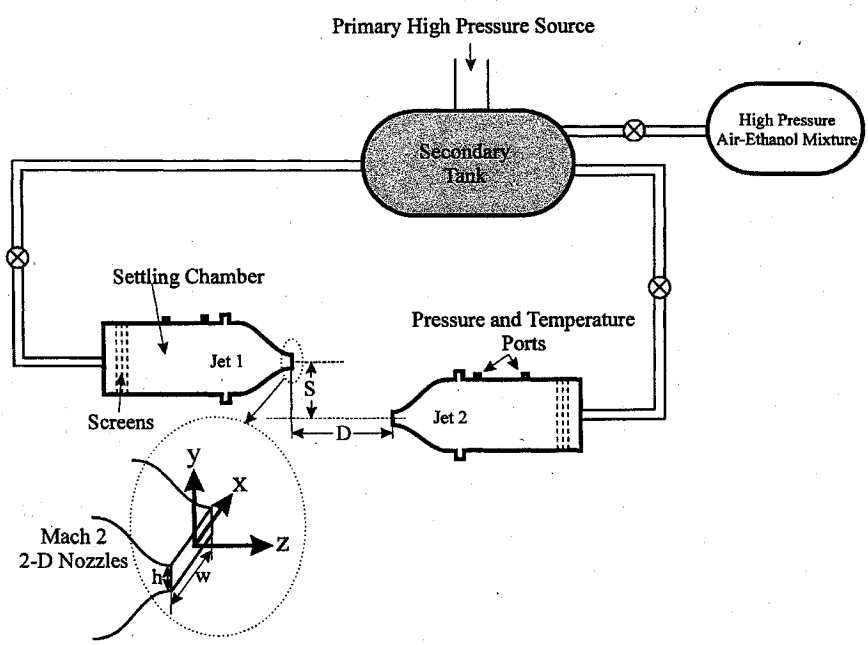

Fig. 1 Schematic of countercurrent test facility.

thus permitting us to effectively control the amount of counterflow between the two shear layers.

Diagnostic Techniques

The experimental program relies on several measurement techniques. The principal diagnostic techniques are as follows: conventional pitot probe surveys, to obtain the mean pitot-pressure profiles and shear layer growth rates; fluctuating pitot and static pressure surveys, using fast response (~50 kHz) pitot and static pressure probes, to obtain turbulence properties (these results are presented in a separate publication[19]); schlieren photography, to provide qualitative information regarding the mean and turbulent characteristics of the flowfield; and flow visualization using planar laser scattering (PLS), also called the laser light sheet technique, to provide nonintegrated images of the turbulent structures.

Pitot Surveys

The small physical scale of the flowfield required the use of an extremely small pitot probe. A pitot probe with a rectangular opening approximately 0.1 mm high and 0.4 mm wide was made by flattening a small diameter stainless steel hypodermic tube. The probe is traversed using a high-resolution indexer/stepper-motor with a step size of 0.0127 mm (0.0005 in.). The combination of the small probe and the high-resolution traversing mechanism allowed for very detailed pitot surveys.

Flow Visualization

A white light spark source with a pulse duration of approximately 10 μs was used in a conventional z-type schlieren system to obtain integrated, instantaneous, and mean images of the shear layer. In all of the images presented in this paper, a horizontal knife edge was used at the cutoff plane to accentuate the gradients in the shear layers.

Two Spectra Physics Nd:YAG lasers (model DCR-11, pulse duration ~10 ns) were used as the source for the PLS flow visualization study. The simultaneously triggered lasers (pulse separation <5 ns, and total energy of approximately 180 mJ/pulse) produced a very thin and very bright light sheet using a combination of two spherical and two cylindrical lenses.[20]

The flowfield was seeded with 99.9% ethyl alcohol (ethanol) with a mass loading of less than 0.1%. Aerosols such as ethanol and water vapor are routinely used to visualize supersonic shear layers; computations by Squires and Eaton[21] have shown that mass loadings of less than 1% have a negligible effect on the turbulent characteristics of the flowfield. Clemens and Mungul[22] conducted a detailed investigation of the behavior of condensed ethanol in supersonic shear layers under similar conditions and concluded that submicron (<0.1 μm) particles accurately track the flow.

In principle, the brightness of a PLS image is proportional to the local fluid density, and thus high-density regions such as those following shock waves appear very bright. In high-temperature zones their may be some evaporation of the droplets that may reduce the image brightness, but this usually occurs for significant temperature jumps such as that across a strong shock wave. Nevertheless, even strong shock waves are still clearly visible as sharp bright lines that are sometimes followed by a local dark region because of the evaporation of part of the ethanol. For moderate to weak shocks the temperature effects are usually not significant, at least to a first order. Hence the PLS technique is ideal for visualizing the shear layer flowfield including any shock waves that might be present.

For an accurate implementation of the PLS technique, it is essential that the flow be uniformly seeded so as not to bias the image intensity. To this end, the high pressure air from the primary storage tanks is first routed through a secondary tank (see Fig. 1). During a PLS experiment, ethanol is simultaneously injected into the secondary tank where it is thoroughly mixed with the high-pressure air supply, thus ensuring uniform seeding of the jet flows.

Both the schlieren and the PLS images were recorded using one of the two available digital charge-coupled device (CCD) cameras: Kodak MegaPlus, Model 4.2, resolution 2048 x 2048 pixels, and Kodak MegaPlus, Model 1.4, resolution 1024 x 1024 pixels. Schlieren and PLS images were also recorded on S-VHS videotape (standard 30-Hz framing rate) using a Panasonic high-resolution (512 x 480 pixels) CCD video camera.

Results and Discussion

To sustain the anticipated elevated turbulence levels, based on the findings of Strykowski et al.,[13] the shear level was maximized by bringing the two opposing flowstreams as close as possible. Furthermore, we also had to ensure that the flowfield, though highly turbulent, was well behaved in the mean. An unsteady (in the time-averaged sense) or pathological shear layer was clearly not desirable. In light of these constraints, several combinations of the streamwise and transverse jet separations (corresponding to S and D, respectively in Fig. 1) were attempted. A sufficiently large and stable mean flowfield was obtained for $S = 12.7$ mm ($S/h \approx 2.5$) and $D = 37.5$ mm ($D/h = 7.5$). This combination, which also corresponds to the flowfield with maximum counterflow and mean shear, serves as our primary test case. For all other cases D was fixed at 37.5 mm, and the amount of counterflow was controlled by adjusting the transverse distance S.

A summary of the test cases and the corresponding measurements is presented in Table 1. A check mark ✓ indicates that a certain type of diagnostic technique was used. As seen in the table, the separation S is incremented by roughly half the nozzle height ($h/2$) between adjacent cases. Larger jet separations were also investigated using flow visualization. However, as the following results will show, incrementing the separation beyond case 4 does not produce significantly different flowfields; hence these cases will not be discussed. Note that the primary test case (i.e., the shear layer with maximum counterflow) corresponds to case 1.

Mean Flowfield

Flow Visualization

A typical time-averaged (average of 30 images) schlieren image corresponding to the primary test case, case 1, is shown in Fig. 2. To get a sense of the physical length scales involved, realize that the jets have a width of 5 mm at the nozzle exit. The schlieren image in Fig. 2 shows the opposing shear layers grazing each other, whereas the mean flowfield appears to be well behaved. In contrast, if the jets are moved any closer, the mean flowfield becomes very unsteady, resulting in a flapping motion of the two jets. A closer look reveals that the width of the shear layer with counterflow is significantly higher than the corresponding shear layer without counterflow. This can be verified by comparing the upper shear layers from both jets, which appear dark, at corresponding axial locations. For example, at roughly 6 mm from each nozzle exit ($z/h \approx 1.2$) the approximate widths of the shear layers have been marked by white lines and the upper shear layer from jet 2 appears to be twice the width of the upper shear layer from jet 1.

The enhanced growth rate in the countercurrent shear layer is further evidenced by the short extent of the potential cores of the jets. The potential core of a jet is defined as the inviscid region between the two shear layers where the average Mach number is nominally constant. In a schlieren image the potential or inviscid core of a jet is usually indicated by the presence of waves. As seen in the schlieren image, the core terminates between $z/h \approx 2$–2.5. This is in sharp contrast to the potential core length of a free jet, where the inviscid cores usually persists eight to ten jet heights downstream. Such a case is presented in Fig. 3, which shows a mean schlieren image of a single jet (jet 1); the lower nozzle is at the relative location for case 1, but the flow has been turned off. The visual shear layer growth

Table 1 Summary of test cases

Case no.	S, mm	Flow visualization		Pitot surveys	
		Schlieren	PLS	Jet centerline	Shear layer
1	12.7	✓	✓	✓	✓
2	15.2	✓	✓	✓	✓
3	17.8	✓	✓	✓	✓
4	20.3	✓	✓	✓	✓
5	22.9	✓	✓	✓	—
6	25.4	✓	✓	—	—

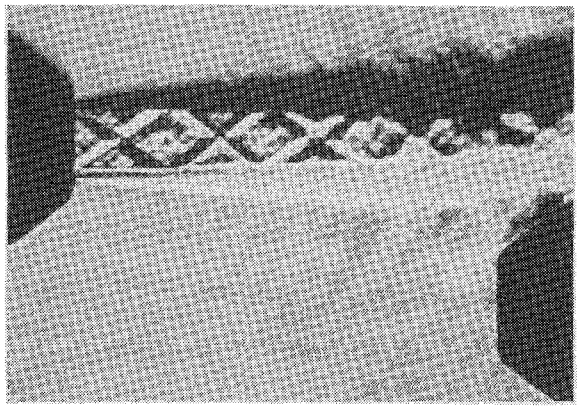

Fig. 3 Time-averaged schlieren image for jet 1 only.

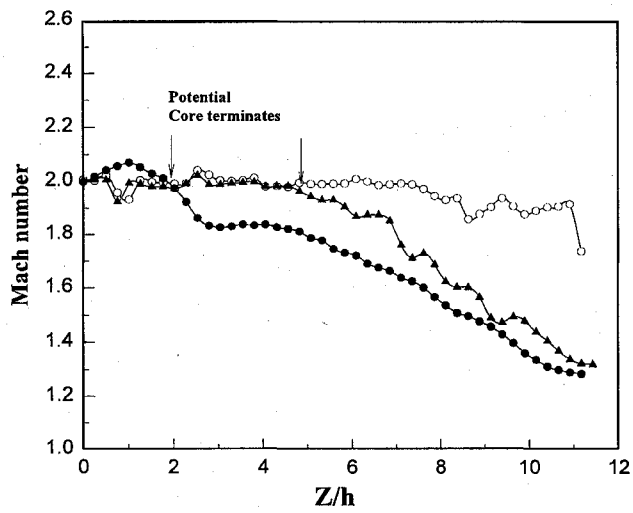

Fig. 4 Centerline, axial Mach number profiles: ○, $S/h = 2.54$ (freejet); ●, $S/h = 2.54$ (case 1); and ▲, $S/h = 3.6$ (case 3).

rate of the free jet lies well within the scatter of published data[2,6,13] for coflowing shear layers. (The graininess is a result of the lower resolution of this image that was digitized from videotape; all other images shown were captured directly via digital cameras.)

Pitot Surveys

The extent of the potential core was quantified by obtaining axial Mach number profiles for cases 1–5. The Mach number was calculated using the measured pitot pressures and assuming constant static pressure (equal to ambient pressure). For the sake of clarity, only the profiles for cases 1 and 3 are plotted in Fig. 4, along with the axial profile for a single jet. (The slight overshoot in the centerline pitot pressure at $z/h \approx 1$ is due to the weak waves seen in Fig. 2. Researchers[7,23] have demonstrated that the presence of weak to moderate compression wave does not alter the global shear layer growth rates.) The potential core for the single jet persists for at least eight jet widths, whereas the cores for counterflowing jets, shown as filled symbols, decay much more rapidly. The approximate locations where the potential cores terminate are marked by arrows. By comparing cases 1 and 3, the effect of varying the counterflow becomes evident.

To further examine this behavior, a plot of the potential core length as a function of jet separation is shown in Fig. 5 where all of the dimensions are normalized by the jet height. In this and all subsequent plots, uncertainty bars have only been indicated for one point. On a given plot such bars are representative of the uncertainty at all points. In Fig. 5, case 1 has the shortest potential core terminating around $z/h \approx 2.2$. Proceeding from cases 1 to 2, an increase in jet separation S results in an increase in the core length. A further increment in S leads to a very dramatic increase in the core length, evident by the break in the plot; additional increments do not affect the core length appreciably. Similar behavior was also visually observed in the mean schlieren images.

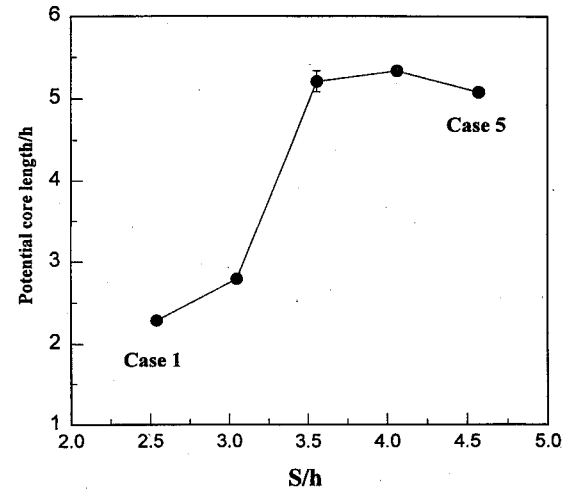

Fig. 5 Effect of jet separation on potential core length.

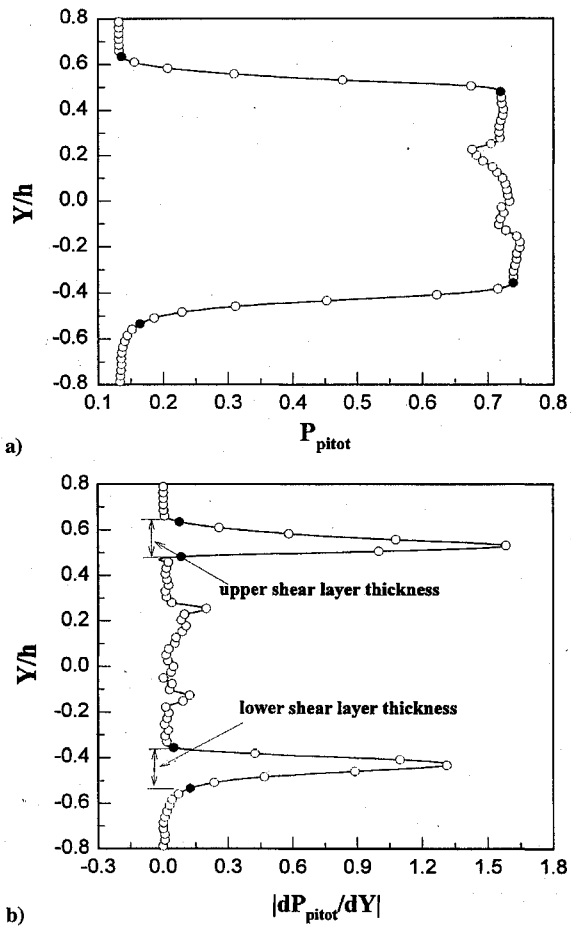

Fig. 6 Shear layer pitot surveys for case 2 with jet 1, and $z/h = 0.5$: a) normalized pitot profile and b) slope profile.

Detailed pitot surveys across the shear layer were also conducted at several streamwise locations to measure the pitot shear layer thickness δ_{pitot} and shear layer growth rate. Instead of using the conventional definition[2] of $0.05\Delta P_{pitot} - 0.95\Delta P_{pitot}$ to estimate δ_{pitot}, a slightly different method is used, as discussed. The accuracy of the standard definition is primarily dependent upon how well the freestream pitot pressures can be defined. This is generally not an issue when the flow is wave free. However, in the presence of waves, even fairly weak ones, the definition of freestream pitot pressure levels becomes more subjective. In support of this, we present Fig. 6a, that shows a pitot pressure profile across jet 1 for case 2 at $z/h = 0.5$. The pitot pressure has been normalized by the settling chamber total pressure. The waves in the potential core lead to a nonuniform pitot

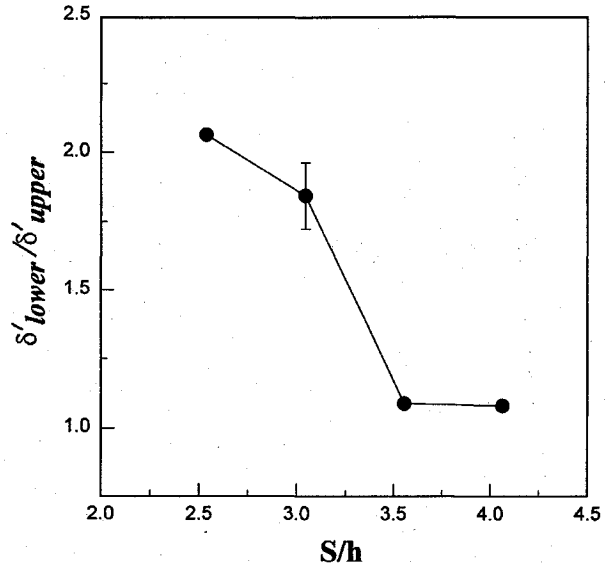

Fig. 7 Shear layer growth ratio of as a function of jet separation (S/h): δ'_{upper}, shear layer without counterflow and δ'_{lower}, shear layer with counterflow.

pressure in the core that may introduce an uncertainty in the pitot thickness definition. We addressed this issue by recognizing that the most distinctive characteristics of shear layers are the steep pressure gradients. Consequently, by plotting the absolute slopes $|dP_{pitot}/dy|$ as a function of position, we can delineate the extent of the shear layer more easily. Such a plot, corresponding to the profile of Fig. 6a, is shown in Fig. 6b. The shear layers are represented by the two hills in the plot. The edges of the shear layer are defined as the points where the absolute change in slope between adjacent points is less than 5% of the maximum slope (the peaks in Fig. 6b).

The validity of this criterion was checked by comparing the growth rates of a free jet shear layer with published data. This definition also proved to be much more robust and more consistent than the conventional approach, especially in regions with waves. The filled symbols in Fig. 6 indicate the shear layer edges picked using this definition. Figure 7 shows a plot of the growth rates as a function of jet separation for cases 1–4. To emphasize the effect of counterflow, the ratio of the lower and upper shear layer growth rates is plotted in the ordinate. Although only data for jet 1 are shown, the mixing layers in both jets behave identically due to the flowfield symmetry. For cases 1 and 2, the lower, countercurrent shear layer grows almost twice as fast as the upper, free shear layer. For a larger S the upper and lower shear layers grow at nearly the same rate. These results further demonstrate the effectiveness of counterflow as a means to significantly enhance shear layer entrainment. The break in the plot between cases 2 and 3 (between $S/h \approx 3$ and 3.6), reminiscent of the behavior seen in Fig. 5, again suggests a minimum threshold in the use of this technique.

One may argue that comparing the behavior of the outer shear layers (those that do not experience counterflow) with the inner shear layers is not justified since the convective Mach numbers of the two shear layers are very different. For example, the upper shear layer of jet 1, with quiescent air on one side and $M_\infty = 2$ flow on the other, has a convective Mach number of approximately 0.83. In contrast, the lower shear layer experiences Mach 2 flow on either side and in opposite directions leading to $M_c \approx 2$. However, in Fig. 7 we do not compare the growth rate of the entire countercurrent shear layer but rather that of the half the shear layer, one that extends from the potential core of the jet to the region at which the velocity goes to zero.

To further clarify this, examine Fig. 8, which shows the velocity profiles across the two jets for cases 1 and 3. The velocities are calculated from the pitot measurements assuming a constant static pressure; rather than representing the exact values they are used here to illustrate a trend. Starting in the middle of jet 1 profile (top) for case 1, we observe that the velocity varies from a maximum of approximately 500 m/s from left to right, to 500 m/s in the opposite direction. In doing so, it goes through a stagnation or zero velocity

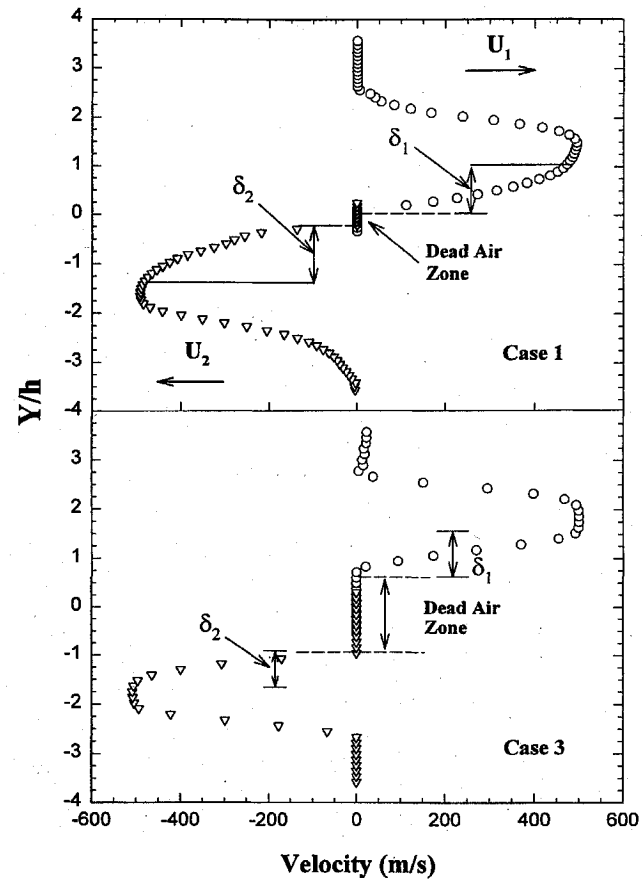

Fig. 8 Velocity profiles across the jets for cases 1 and 3: ○, jet 1 and ▽, jet 2.

region marked as the dead air zone in the figure. In determining the countercurrent shear layer growth rates shown in Fig. 7, the shear layer thickness has been defined as the region extending from the potential core to the dead air zone. Consequently, this half shear layer, indicated as δ_1 in Fig. 8, with Mach 2 flow on one side and zero velocity on the other, has approximately the same convective Mach number as the upper shear layer. Also note that due to the flow symmetry the growth rate of the upper half of the countercurrent shear layer δ'_1 is the same as the lower half of the shear layer δ'_2.

A qualitative examination of Fig. 8 affords further insight into the behavior of the present flowfield. For case 1 the dead air zone is very small, essentially a stagnation streamline, and the flow smoothly reverses direction through this region. In contrast, for case 3, this region—where the mean velocity is zero—is fairly sizable extending approximately one jet height in the y direction. Intuition suggests that although the mean velocity in this zone is essentially zero, for small jet separations the flow would be highly turbulent. This is indeed the case, as demonstrated in a subsequent discussion of the turbulent flow properties. Consequently even though the convective Mach number of the upper shear layer (thickness δ_1) is defined in terms of the mean velocity in this region, the dynamics of the shear layer flow are determined by the fact that the entire countercurrent shear layer is bounded by freestreams in opposite directions, making this region highly turbulent. Hence, the growth rates in the countercurrent half shear layer at comparable M_c are substantially higher. As the jet separation is increased, the size of the dead air zone increases, and the turbulence levels decline[19] until a limit is reached beyond which both jets behave independently of each other. Beyond this critical separation S, the inner shear layers no longer feel the effect of counterflow and behave in the same manner as the outer shear layers. As previously discussed, this appears to happen between cases 2 and 3.

In the context of the preceding discussion, to study the $M_c \approx 2$ countercurrent shear layer it may be useful to examine the behavior of the entire countercurrent shear layer, δ_{total}, shear layer that is bounded by Mach 2 flow on either side. The behavior of this shear

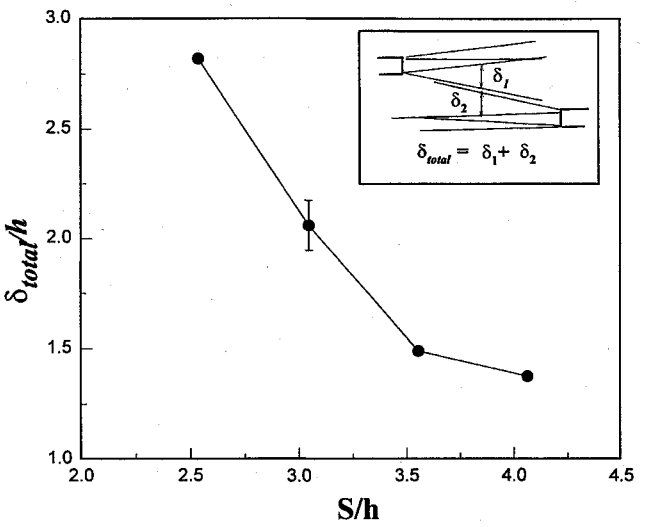

Fig. 9 Total shear layer thickness as a function of jet separation at $z/h = 3.5$.

layer, defined as the sum of two half shear layers δ_1 and δ_2 (see Fig. 8), is shown as a function of jet separation in Fig. 9. The inset in the plot should serve to further clarify the definition of δ_{total}. This figure represents measurements made at $z/h = 3.5$, but the same trends are observed at any streamwise location. As expected, case 1 has a substantially higher shear layer thickness, and the curve begins to flatten out for cases 3 and 4, reflecting the reduced influence of counterflow at higher separations.

We now briefly discuss the possible mechanisms that may explain this behavior. As mentioned in the introduction, Strykowski et al.[13] also observed a substantial increase in the mixing rates of axisymmetric countercurrent shear layers. More importantly, their study revealed that counterflow was only effective for values of R above a critical threshold. Prompted by their experimental results the authors explored the stability characteristics of the countercurrent shear layer using spatiotemporal theory. Their analysis revealed that for $M_c < 1$ the shear layers become increasingly stable with increasing M_c. However, for $M_c > 1$ the opposite trend is observed; namely, the countercurrent shear layer becomes increasingly unstable and more susceptible to a transition to absolute instability. Correspondingly, the theoretical critical level of counterflow required to achieve an absolutely unstable flowfield also decreases with increasing M_c for $M_c > 1$.

The trends observed in our experiments are qualitatively very similar to the experimental and theoretical results of Strykowski et al.[13] Specifically, we find that above a certain jet separation—in essence, below a certain amount of counterflow—the countercurrent shear layers did not experience an increase in growth rates. Once a critical counterflow value is exceeded, in our case, when $S < 17.8$ mm (case 3), the countercurrent shear layer grows much more rapidly. In addition, for small jet separations, the amount of counterflow in the present flowfield far exceeds the critical levels, predicted by spatiotemporal theory, needed to support an absolutely unstable flow. Based on these observations and on the similarities to theoretical[14] and experimental[24,25] studies at lower speeds, we believe that circumstantial evidence suggests that a transition from convective to absolute instability, ultimately leading to a globally unstable flow, may be responsible for the elevated mixing rates in the present countercurrent shear layer. The transition to global instability appears to be primarily a nonlinear function of the jet spacing and occurs between cases 2 and 3. A more rigorous proof of the instability mechanism would at a minimum require very detailed measurements of the unsteady characteristics and the response of the flowfield to moderate external forcing.[15]

If global instability is indeed the mechanism governing the dynamics of the present shear layer, then this flow is fundamentally different from a coflowing shear layer governed by convective instability. Consequently, the validity of conventional analysis techniques based upon coflowing studies may not always be applicable. For instance, the practice of normalizing the compressible growth rates by incompressible values may not be valid, especially at high levels of counterflow. As an example, for case 1 where $U_2/U_1 \approx -1$, the standard definition[2] yields an infinite incompressible pitot growth rate, a value that clearly cannot be used to normalize the compressible growth rates. Another significant consequence of the globally unstable nature of the shear layer is the fact that the limitations on its size are now due to the physical boundary conditions, in this case the finite height of the jet potential core. In other words, we suspect that, for the globally unstable flowfields of cases 1 and 2, an increase in jet height would lead to a proportional increase in δ_{total} (Fig. 9). For such flows, the convective Mach number may no longer be a relevant parameter.

One final note regarding the suitability of using an intrusive pitot probe in a potentially global flowfield should be made. Sreenivasan et al.[26] investigated the effect of intrusive probes on the dynamics of low-speed variable density jets. They found the region of influence, defined as the streamwise distance from the nozzle exit over which the probe can influence the stability characteristics, to decrease with increasing jet Mach number. An extrapolation of their results to the present flow conditions suggests that the region of influence in this flow is much less than the first downstream station at which probe surveys are conducted. This assertion is further supported by the good agreement between our visual (nonintrusive) and pitot growth rate measurements.

Before discussing the turbulent properties, we briefly summarize the results presented so far. Using a variety of different methods, namely, potential core length (Fig. 5), shear layer growth rates (Fig. 7), and total shear layer thickness (Fig. 9), we have demonstrated that counterflow has a profound effect on shear layer growth rates. The shear layers for case 1, and to a lesser degree case 2, grow or entrain fluid at significantly higher rates. We believe that this may be due to a fundamental difference in the dynamics of the shear layers and suggest that a transition from convective to global instability may occur for 17.8 mm $> S >$ 15.2 mm (between cases 2 and 3). Based upon this evidence, we propose that case 1 ($M_c \approx 2$ countercurrent shear layer) and case 2 may be governed by global instability, whereas case 3 (and onward) are governed by the convective instability present in conventional coflowing shear layers.

Turbulent Flowfield

We expect that the increased entrainment of the countercurrent shear layers is due to the modification of the large-scale turbulent

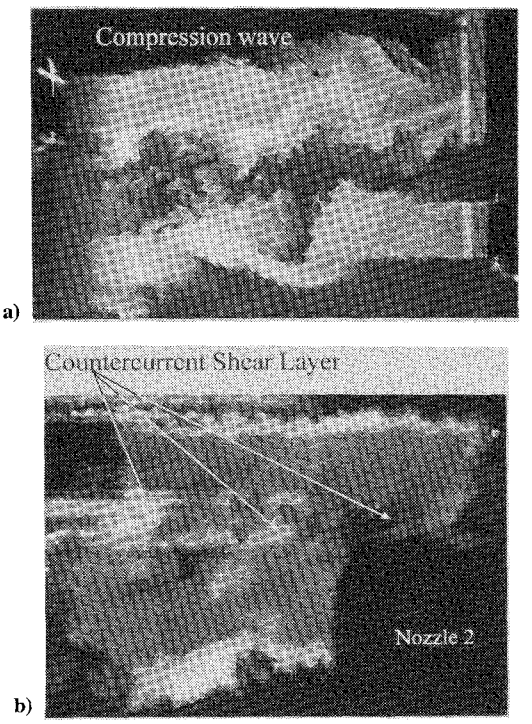

Fig. 10 Instantaneous PLS images of the countercurrent shear layer: a) side view and b) cross-sectional view.

structures in the shear layer. Consequently, the turbulent flowfield was examined using the PLS technique. Figure 10a depicts a side view, and Fig. 10b shows a diametral view (cross-sectional view in the x–y plane) of the turbulent flowfield corresponding to case 1. Each image is exposed by a single laser pulse (duration <10 ns), thus essentially freezing the structure, and is representative of the turbulent flowfield for this case.

Both images show the presence of large, highly convoluted, violent structures that in many instances span the entire region between the jet centerlines. In contrast, the structures in the outer shear layers, those without counterflow, are relatively small. The discrepancy between the length scales of the large-scale structures is especially evident in the diametral PLS view shown in Fig. 10b. The free shear layer structures are very small with relatively little spatial coherence, whereas those in the countercurrent layer are large, highly convoluted, and three dimensional. An interesting result of the excursions of these large-scale structures into the primary jet flows is the formation of compression waves around the structures. One such wave has been marked in Fig. 10a. The size and the frequency of appearance of the large-scale structures declined as the jet separation was increased. Fluctuating pitot pressure measurements were also conducted, using a fast response pitot probe, to quantify the turbulence intensities.[19] For case 1, the rms levels in the countercurrent shear layer are almost an order of magnitude greater than those in the free shear layer, and the fluctuating intensity decreases with increasing jet separation. These trends are consistent with the mean flowfield measurements and suggest that the higher turbulence intensities in the countercurrent shear layer are primarily responsible for the enhanced growth rates.

Eddy Shocklets

As stated in the Introduction, computations[17] of highly turbulent flowfields have indicated the presence of eddy shocklets. However, to the authors' knowledge such eddy shocklets have never been observed experimentally, perhaps due to the strict requirements, as suggested by Lee et al.,[17] necessary for the formation of readily observable eddy shocklets. These include a primarily two-dimensional flowfield with a high turbulent Reynolds number and a high turbulent Mach number, conditions not easily simulated experimentally. We believe that in the present study the flowfield with maximum counterflow (case 1) possesses all of the properties stated earlier. The mean flowfield is nominally two dimensional, and the large length scales of the turbulent structures (Fig. 10), the very high fluctuating pressure intensities,[19] together with the high unit Reynolds number, result in a high turbulent Reynolds number (estimated to be >30) and a high turbulent Mach number.

Figure 10 clearly shows that the PLS technique is capable of detecting the existence of even weak compression waves. As a logical extension we assume that eddy shocklets, if present, would be detectable using this technique, provided we have sufficient resolution. Utilizing the high-resolution camera (2048 × 2048 pixels) at the highest possible magnification, we examined the flowfield in exhaustive detail for evidence of eddy shocklets. Figure 11 shows two examples representative of the many PLS images that were examined. The magnification of the image shown in the figure is approximately 7.5 μm/pixel, the maximum feasible with the present hardware. The streamwise widths of the regions shown in Figs. 11a and 11b are approximately $3h$ and $2.5h$ (1.46 and 1.26 cm), respectively. As a scale reference, a line of length $h/2$ (2.5 mm) has also been drawn on these images.

According to the computational results,[17] an eddy shocklet satisfies the shock jump conditions and must therefore appear as a shock wave would in the PLS images. This implies that an eddy shocklet would appear as a distinct and sharp line in the shear layer with an abrupt change in the image brightness across it. To the best of our ability we were unable to observe any such eddy shocklets. We must caution the reader not to confuse the presence of shocklets or compression waves in the jet flows with eddy shocklets. Figure 10 shows ample evidence of compression waves in the jet flows (see earlier discussion of Fig. 10a). However, an eddy shocklet is generated because of the locally supersonic (relative to the surrounding flow) convection of the large eddies and must be present in the shear layer.

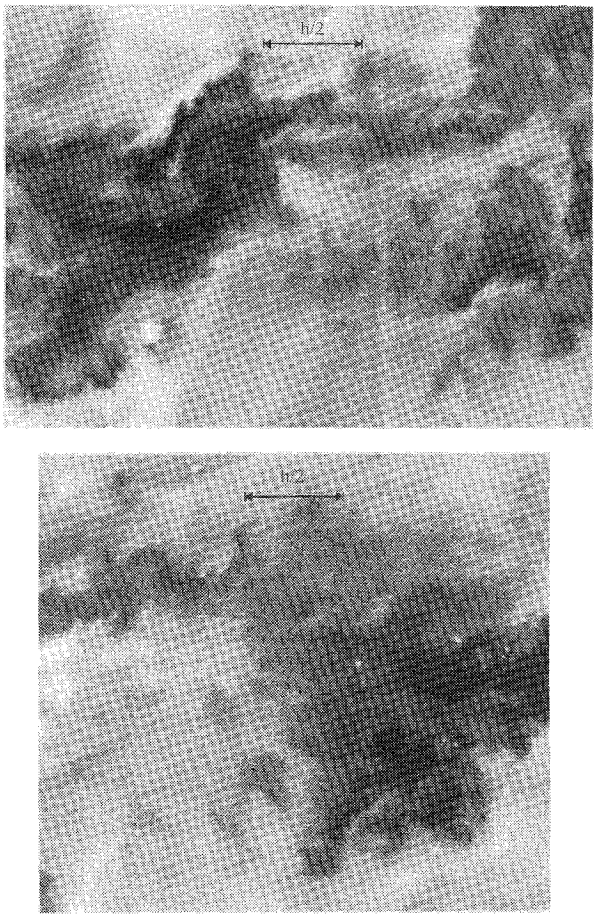

Fig. 11 Magnified instantaneous PLS images of the countercurrent shear layer in search of eddy shocklets.

In the context of this definition, we contend that no eddy shocklets were visualized in the present flowfield.

This does not necessarily preclude the presence of eddy shocklets. However, we can confidently state that, in a carefully conducted flow visualization study with extremely high image resolution, we did not observe the presence of eddy shocklets. If such shocklets are present, their length scales are likely to be smaller than the resolution of the PLS images. In such a case, one must question the significance of these structures on the overall fluid dynamics of the flow.

Conclusions

We have successfully demonstrated the ability to generate a countercurrent shear layer at a very high convective Mach number. The entrainment characteristics of this shear layer are found to be much more favorable than those of coflowing shear layers. The enhanced mixing is primarily because of the presence of large, convoluted, three-dimensional turbulent structures not observed in compressible coflowing shear layers. Based upon the similarity between this and previous studies at lower convective Mach numbers, we suggest that the present flowfield may be governed by global rather than convective instability thus making it very different than the conventional coflowing shear layers. We also propose that conventional parameters and analysis techniques, primarily based upon coflowing shear layer studies, may not always be applicable for counterflowing shear layers. Finally, and most importantly, the efficient mixing of this countercurrent shear layer, especially for such highly compressible flows, makes this flow very attractive from a practical perspective.

Acknowledgments

The authors gratefully acknowledge the support of NASA (NAG 2930) in conducting this research. We would like to thank P. J. Strykowski from the University of Minnesota for his invaluable advice. We would also like to thank the engineering staff at

the laboratory, especially J. Taylor and R. Dawkins, for their timely response to our untimely requests, and E. Barber and D. Forliti for their assistance in data acquisition.

References

[1]Brown, G. L., and Roshko, A. R., "On Density Effects and Large Structure in Turbulent Mixing Layers," *Journal of Fluid Mechanics*, Vol. 64, No. 4, 1974, pp. 775–781.

[2]Papamoschou, D., and Roshko, A. R., "The Compressible Turbulent Shear Layer; An Experimental Study," *Journal of Fluid Mechanics*, Vol. 197, Dec. 1988, pp. 453–477.

[3]Bogdanoff, D. W., "Compressibility Effects in Turbulent Shear Layers," *AIAA Journal*, Vol. 21, No. 6, 1983, pp. 926, 927.

[4]Papamoschou, D., "Structure of the Compressible Turbulent Shear Layer," *AIAA Journal*, Vol. 29, No. 5, 1991, pp. 680, 681.

[5]Bunyajitradulya, A., and Papamoschou, D., "Acetone PLIF Imaging of Turbulent Shear-Layer Structure at High Convective Mach Number," AIAA Paper 94-0617, Jan. 1993.

[6]Clemens, N. T., and Mungul, M. G., "Two-and-Three-Dimensional Effects in the Supersonic Mixing Layer," *AIAA Journal*, Vol. 30, No. 4, 1992, pp. 973–981.

[7]Shau, Y. R., Dolling, D. S., and Choi, K. Y., "Organized Structure in a Compressible Turbulent Shear Layer," *AIAA Journal*, Vol. 31, No. 8, 1993, pp. 1398–1405.

[8]Jackson, T. L., and Grosch, C. E., "Inviscid Spatial Stability of a Compressible Mixing Layer," *Journal of Fluid Mechanics*, Vol. 208, Nov. 1989, pp. 609–637.

[9]Papamoschou, D., "Structure of the Compressible Turbulent Shear Layer," AIAA Paper 89-0126, Jan. 1989.

[10]Samimy, M., Zaman, K. B. M. Q., and Reeder, M. F., "Supersonic Jet Enhancement by Vortex Generators," AIAA Paper 91-2263, July 1991.

[11]Naughton, J. W., "The Enhancement of Turbulent Compressible Mixing via Streamwise Vorticity," Ph.D. Dissertation, Dept. of Mechanical Engineering, Pennsylvania State Univ., University Park, PA, May 1993.

[12]Lepicovsky, J., Ahuja, K. K., Brown, W. H., and Burrin, R. H., "Coherent Large Scale Structure in High Reynolds Number Supersonic Jets," *AIAA Journal*, Vol. 25, No. 11, 1987, pp. 1419–1425.

[13]Strykowski, P. J., Krothapalli, A., and Jendoubi, S., "The Effect of Counterflow on the Development of Compressible Shear Layers," *Journal of Fluid Mechanics* (to be published); see also AIAA Paper 93-3260, July 1993.

[14]Pavithran, S., and Redekopp, L. G., "The Absolute-Convective Transition in Subsonic Mixing Layers," *Physics of Fluids A*, Vol. 1, No. 10, 1989, pp. 1736–1739.

[15]Huerre, P., and Monkewitz, P. A., "Local and Global Instabilities in Spatially Developing Flows," *Annual Review of Fluid Mechanics*, Vol. 22, 1990, pp. 473–537.

[16]Chomaz, J. M., Huerre, P., and Redekopp, L. G., "Bifurcations to Local and Global Modes in Spatially-Developing Flows," *Physics Review Letters*, Vol. 60, No. 1, 1988, pp. 25–28.

[17]Lee, S., Lele, S. K., and Moin, P., "Eddy Shocklets in Decaying Compressible Turbulence," *Physics of Fluids*, Vol. 3, No. 4, 1991, pp. 657–664.

[18]Zeman, O., "Dilatation Dissipation: The Concept and Application in Modeling Compressible Mixing Layers," *Physics of Fluids*, Vol. 2, No. 2, 1990, p. 178.

[19]Alvi, F. S., and Krothapalli, A., "Fluctuating Pressure Measurements in a Highly Compressible Countercurrent Turbulent Shear Layer," AIAA Paper 95-2175, June 1995.

[20]Alvi, F. S., and Settles, G. S., "Physical Model of the Swept Shock Wave/Boundary-Layer Interaction Flowfield," *AIAA Journal*, Vol. 30, No. 9, 1992, pp. 2252–2258.

[21]Squires, K., and Eaton, J., "Particle Response and Turbulence Modification in Isotropic Turbulence," *Physics of Fluids A*, Vol. 2, No. 7, 1990, pp. 1191–1203.

[22]Clemens, N. T., and Mungul, M. G., "A Planar Mie Scattering Technique for Visualizing Supersonic Mixing Flows," *Experiments in Fluids*, Vol. 11, May 1991, pp. 175–185.

[23]Wishart, D. P., and Krothapalli, A., "On the Structure of a Heated Supersonic Jet," AIAA Paper 94-0666, Jan. 1994.

[24]Strykowski, P. J., and Wilcoxon, R. K., "Mixing Enhancement Due to Global Oscillations in Jet with Annular Counterflow," *AIAA Journal*, Vol. 31, No. 3, 1993, pp. 564–570.

[25]Strykowski, P. J., and Niccum, N. L., "The Stability of Countercurrent Mixing Layers in Circular Jets," *Journal of Fluid Mechanics*, Vol. 227, June 1991, pp. 309–343.

[26]Sreenivasan, K. R., Raghu, S., and Kyle, D., "Absolute Instability in Variable Density Round Jets," *Experiments in Fluids*, Vol. 7, April 1989, pp. 309–317.